Journal of Catalysis **195,** 169–179 (2000)
doi:10.1006/jcat.2000.2983, available online at http://www.idealibrary.com on IDEAL®

The Interaction between NO and CO on Rh-Loaded CeO_x(111)

D. R. Mullins,[1] Lj. Kundakovic,[2] and S. H. Overbury

Oak Ridge National Laboratory, Oak Ridge, Tennessee 37831-6201

Received March 28, 2000; revised June 27, 2000; accepted June 28, 2000

We have used SXPS and TPD to probe the interactions between CO and NO on ceria-supported Rh model catalysts (Rh/CeO_x). On a highly reduced ceria substrate the only desorption products were CO and N_2. No NO or CO_2 were observed, as have been seen on Rh single-crystal surfaces. The desorption profiles of the CO and N_2 were much different than the desorption spectra from CO or NO adsorbed alone, suggesting a strong interaction between the CO and NO. C 1*s*, N 1*s*, and O 1*s* photoemission spectra were recorded to determine the surface intermediates. There is little interaction between the CO and NO below 400 K. Near 400 K the CO reacts with atomic N from dissociated NO to form OCN. The isocyanate dissociates near 600 K, producing desorbed CO and carbon–nitrogen species, C_XN_Y, on the surface. The C_XN_Y decomposes above 700 K to produce CO and N_2. The reduced ceria substrate introduces several reaction paths that help promote reactions not ordinarily observed on pure Rh. The reduced ceria removes O from the Rh. This inhibits the formation of CO_2 and promotes OCN formation. The reduced ceria also promotes the dissociation of CO. After dissociation, the O is removed by the ceria and the atomic C and N react, forming C_XN_Y.

Key Words: **CO; carbon monoxide; NO; nitric oxide; OCN; isocyanate; ceria; CeO_2; rhodium; X-ray photoelectron spectroscopy; temperature-programmed desorption.**

INTRODUCTION

The catalytic reduction of NO by CO is one of the principal reactions involved in automotive exhaust catalysts. The mechanism and kinetics of this reaction have been the subject of numerous studies (1–7) and the literature has been recently reviewed (8). The primary elementary reaction steps are generally accepted to consist of the following (8):

$$NO(g) \Leftrightarrow NO(a) \quad [1.1]$$

$$CO(g) \Leftrightarrow CO(a) \quad [1.2]$$

$$NO(a) \Rightarrow N(a) + O(a) \quad [1.3]$$

$$2N(a) \Rightarrow N_2(g) \quad [1.4]$$

$$CO(a) + O(a) \Rightarrow CO_2(g). \quad [1.5]$$

Under UHV conditions, only the surface intermediates and gaseous products listed above have been identified following reaction on single-crystal and polycrystalline Rh surfaces. Other reaction steps, such as,

$$CO(a) + N(a) \Rightarrow OCN(a) \quad [1.6]$$

$$N(a) + NO(a) \Rightarrow N_2O(a), \quad [1.7]$$

have also been identified at elevated pressures (4, 9, 10).

When the Rh is supported on reduced cerium oxide, referred to in the following as CeO_x, several other elementary steps have been identified. From the adsorption of CO on Rh supported on reduced ceria, Rh/CeO_x, the following reactions have been identified (11–13):

$$CO(a) \Rightarrow C(a) + O(a) \quad [1.8]$$

$$O(a) + Ce_2O_3 \Rightarrow 2CeO_2. \quad [1.9]$$

Inclusion of these reactions into the framework established in reactions [1.1]–[1.7] may alter the observed reaction products and surface intermediates. In addition, the reduced ceria substrate may also have a profound influence on the kinetics and equilibria associated with the elementary steps.

In this study we report that when NO and CO are coadsorbed on Rh/CeO_2, the results are fully explained by reactions [1.1]–[1.5] and are consistent with what has been observed on other Rh surfaces. However, if the ceria substrate is reduced, there is no CO_2 formed, but a number of new surface intermediates are identified. These intermediates are assigned as OCN, CN, and C_XN_Y. The reaction pathway may be different, depending on whether CO + NO, CO + N, or C + NO are considered. Each of these possibilities is examined separately.

2. EXPERIMENTAL

The experiments were performed in two different UHV chambers (14). The temperature-programmed desorption

[1] To whom correspondence should be addressed. Oak Ridge National Laboratory, P.O. Box 2008, MS 6201, Oak Ridge, TN 37831-6201. E-mail: mullinsdr@ornl.gov. Fax: 865-576-5235.

[2] Current address: Massachusetts Institute of Technology, E25-342, 77 Massachusetts Avenue, Cambridge, MA 02139.

0021-9517/00

(TPD) experiments were performed in a chamber at ORNL. The temperature was ramped at 3 K/s and the sample was biased −70 V to prevent electron-stimulated reactions. Soft X-ray photoelectron spectroscopy (SXPS) was performed in a chamber at the National Synchrotron Light Source. Experiments were conducted on beamlines X1B and U12A. C 1*s* spectra were recorded using 530-eV excitation on X1B and 405-eV excitation on U12A. N 1*s* spectra were recorded using 550- and 525-eV excitation on X1B and U12A, respectively. O 1*s* spectra were recorded using 600-eV excitation. The instrumental resolution was better than 0.5 eV on both beamlines.

CeO_x(111) films were grown *in situ* on Ru(0001) as previously described (15). The ceria films were estimated to be ca. 5-nm thick based on the attenuation of the Ru 3*d* XPS intensity. The oxidation state of the Ce was controlled in two different ways. In the XPS experiments a fully oxidized CeO_2(111) film was deposited at 700 K. The oxygen pressure was then reduced and additional ceria was deposited. After deposition the sample was annealed to 900 K. In the TPD experiments a fully oxidized film was deposited at 700 K. The sample was then sputtered briefly with Ne^+ ions, which preferentially removes oxygen. The sample was then annealed to 900 K to remove sputter damage (15). The average oxidation state was determined by the Ce 3*d*, Ce 4*d*, or valance band photoemission spectra (16). All ceria films used in this study were substantially reduced. The films used in the XPS studies were 80% Ce^{3+}/20% Ce^{4+}. The films in the TPD experiments were 75% Ce^{3+}/25% Ce^{4+}.

Rh was deposited from a resistively heated evaporative source while the sample was maintained at 300 K. After deposition the sample was heated to 800 K. The same Rh coverage was used for all TPD experiments and for all SXPS experiments. The relative amount of Rh between the TPD and XPS experiments is not known precisely but is believed to be similar. The Rh coverage was estimated to be 5×10^{14} cm^{-2} ($\pm$50%) based on the Rh 3*d* SXPS intensity compared to the Ru 3*d* SXPS intensity for clean Ru, the attenuation of the Ce 4*d* SXPS intensity following Rh deposition, and the CO TPD intensity from the deposited Rh compared to CO from clean Ru(0001).

$^{15}N^{16}O$ and $^{13}C^{16}O$ (Cambridge Isotope Labs) were adsorbed from separate directional dosers (14) in the TPD experiments. Unless otherwise indicated, the gases were dosed to ensure saturation; i.e., further exposure resulted in no changes in the SXPS or TPD spectra. The typical exposure was approximately equal to 20 L. The labeled isotopes allowed CO to be differentiated from N_2 in the TPD spectra. It also separated the relatively weak desorption signals from a background signal at Mass 28. The CO contained ca. 10–15% $^{13}C^{18}O$. This fortuitous contaminant enabled us to do isotopic mixing studies in the desorbing species.

3. RESULTS

3.1. CO or NO Adsorbed at 200 K

The adsorption of CO (13) or NO (17) adsorbed separately on Rh/CeO_x(111) has been reported previously and is summarized here as a reference for the co-adsorption experiments. Thermal desorption spectra following CO or NO exposure at 200 K are shown in Figs. 1a and 1b, respectively. CO, NO, and N_2 are the only desorption products observed. The CO desorbs in two weak low-temperature states centered at 240 and 390 K and an intense state at 660 K. The low-temperature states result primarily from the desorption of undissociated CO on Rh. The high-temperature state results from the recombination of dissociated CO. This assignment is evident from the comparison of the desorption of $^{13}C^{16}O$ and $^{13}C^{18}O$. ^{18}O is only contained in the desorption of undissociated $^{13}C^{18}O$. After dissociation the ^{18}O from the dissociated CO rapidly exchanges with the ^{16}O contained in the ceria. When the C and O recombine, the resulting CO contains primarily ^{16}O (12).

The species adsorbed on the surface after CO was adsorbed at 200 K and then annealed to progressively higher

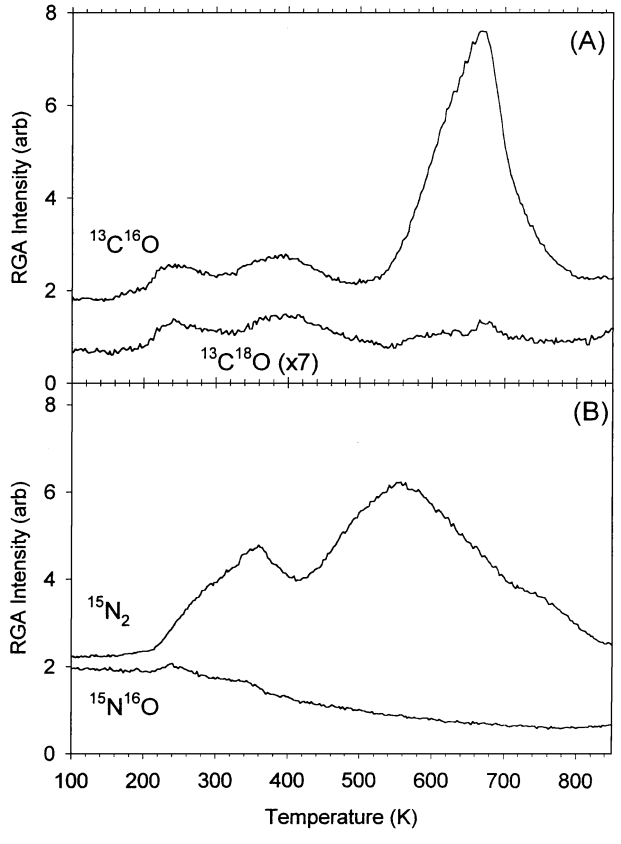

FIG. 1. Thermal desorption spectra from large exposures of (A) $^{13}C^{16}O$ or (B) $^{15}N^{16}O$ adsorbed on Rh/CeO_x at 200 K. The $^{13}C^{18}O$ desorption in (A) resulted from a contaminant in the $^{13}C^{16}O$. The $^{13}C^{18}O$ desorption is indicative of undissociated CO desorption.

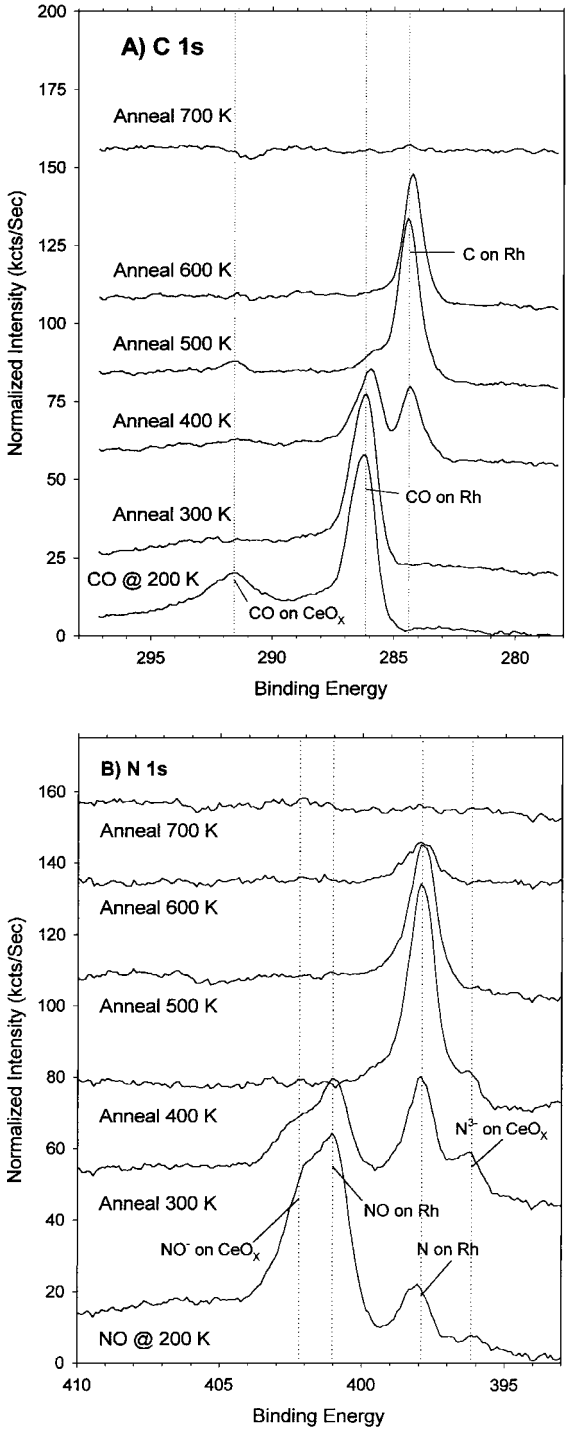

FIG. 2. Core level photoemission spectra for CO or NO adsorbed separately on Rh/CeO_x at 200 K and then annealed for 30 s at progressively higher temperatures as indicated. (A) C 1*s* spectra for CO. (B) N 1*s* spectra for NO.

temperatures were determined from C 1*s* SXPS spectra shown in Fig. 2a. The C 1*s* states resulting from the adsorption of CO have been assigned previously (13). The broad feature at 291.6 eV is assigned to CO adsorption on CeO_x and results from either a carbonate or carboxylate species. The peak at 286.3 eV is assigned to molecular CO on Rh. The peak position shifts to a slightly lower binding energy as the CO coverage decreases at higher temperatures. The peak at 284.4 eV first appears after the sample is annealed to 400 K. This feature is assigned to atomic C on Rh that results from the dissociation of CO. All C 1*s* peaks are gone after the sample is annealed to 700 K.

The desorption of N_2 shown in Fig. 1b contains contributions from the dissociation of NO on CeO_x and NO on Rh/CeO_x. The desorption between 240 and 400 K results primarily from the dissociation and recombination of NO^- on CeO_x (18). The desorption above 400 K is primarily from the recombination of N from dissociated NO on Rh/CeO_x. A small amount of N_2 results from the recombination of N^{3-} from the CeO_x at 500 K (18).

The N 1*s* spectrum following NO adsorption at 200 K (Fig. 2b) is more complex than the C 1*s* spectra for CO because NO interacts more strongly than CO with CeO_x. In addition, the peaks that result from the adsorption of NO on CeO_x overlap with the peaks that result from the adsorption of NO on Rh. Two peaks in Fig. 2b are assigned to states on CeO_x and two are assigned to states on Rh. The peak at 402.2 eV is assigned to NO^- on CeO_x. The feature that appears at 396.2 eV after annealing to 300 K is from N^{3-} on CeO_x. NO on Rh produces a peak at 401.1 eV. After dissociation of the NO on Rh, atomic N on Rh is seen at 398.0 eV.

The NO^- on CeO_x dissociates and mostly desorbs as N_2 between 200 and 400 K. This can be seen in the decrease in NO^- with only a small increase in N^{3-}. The NO on the Rh dissociates but does not desorb at low temperature, resulting in a decrease in NO/Rh and an increase in N/Rh.

3.2. CO and NO Adsorbed at 200 K

CO and NO compete for sites on Rh. If NO is adsorbed first, no CO uptake is observed in the C 1*s* spectrum after subsequent CO exposure. Similarly, if CO is absorbed first, the resulting N 1*s* spectrum following NO exposure indicates that NO only adsorbed on the CeO_x.

CO and NO can be co-adsorbed at 200 K if a subsaturation coverage is produced by one adsorbate and then the other gas is adsorbed. An NO exposure equivalent to ca. 2 L was made at 200 K followed by a saturation exposure of CO at 200 K. CO and N_2 are primarily evolved during the thermal desorption as shown in Fig. 3. Only a trace of CO_2 and no cyanogen, C_2N_2, were observed. NO desorption cannot be determined uniquely because of the overlap between $^{15}N^{16}O$ and $^{13}C^{18}O$. However, the Mass 31 profile matches very closely the Mass 29 ($^{13}C^{16}O$) profile between 200 and 300 K. The intensity ratio between Mass 29 and Mass 31 is similar to what is seen in Fig. 1. Therefore, we are confident that most, if not all, of the desorption at Mass 31 is from $^{13}C^{18}O$ and not $^{15}N^{16}O$.

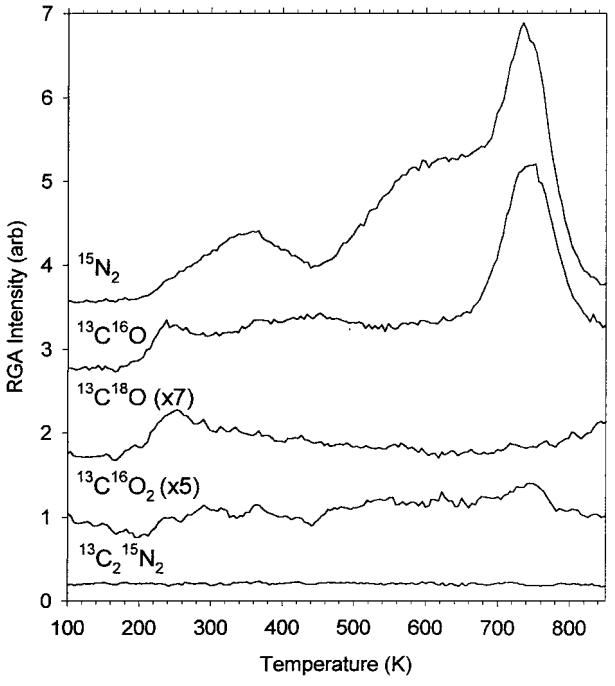

FIG. 3. Thermal desorption spectra following the adsorption of sub-monolayer amounts of $^{15}N^{16}O$ and $^{13}C^{16}O$ on Rh/CeO_x. The $^{15}N^{16}O$ was adsorbed first at 200 K and then followed by $^{13}C^{16}O$ at 200 K. The $^{13}C^{18}O$ desorption is indicative of undissociated CO desorption.

CO desorbs primarily in a well-defined peak at 740 K. A broad plateau that extends from 240 to 650 K precedes this peak. The $C^{13}O^{18}$ desorption indicates that only the desorption near 250 K is from nonrecombinative CO. The biggest effect of the co-adsorption is that the high-temperature, recombinative CO state is sharper and shifts to higher temperature when NO is co-adsorbed (compare Fig. 1a). The N_2 desorption also shows a sharp, intense feature near 730 K that is not observed in the absence of CO (Fig. 1b). The lower temperature N_2 desorption near 340 and 550 K occur in the absence of CO (See section 3.1).

C 1*s* spectra are shown in Fig. 4a following the adsorption of CO on a sub-monolayer coverage of NO at 200 K and also after subsequently annealing to progressively higher temperatures. C/Rh, CO/Rh, and CO/CeO_x are seen at 284.3, 286.4, and 291 eV, respectively. A number of new features appear at temperatures above 400 K. The C 1*s* peak positions and assignments are summarized in Table 1. The rationale for these assignments will be presented in the Discussion (section 4.1).

Isocyanate, OCN, appears at 289.7 eV after the sample is annealed to 400 K. The molecular CO/Rh also decreases in intensity and shifts to lower binding energy and C/Rh begins to emerge. OCN increases in intensity at 500 K and then disappears at 600 K. Another new peak appears at 285.2 eV after annealing to 500 K. There is also increased intensity between 286 and 288 eV but it is not possible to reliably resolve this signal into individual states. As the temperature is increased, the intensity between 286 and 288 eV increases and, based on a comparison with the spectrum at 700 K, can be assigned to two states at 286.8 and 287.4 eV. The states that remain above 600 K are assigned to carbon–nitrogen compounds, C_XN_Y.

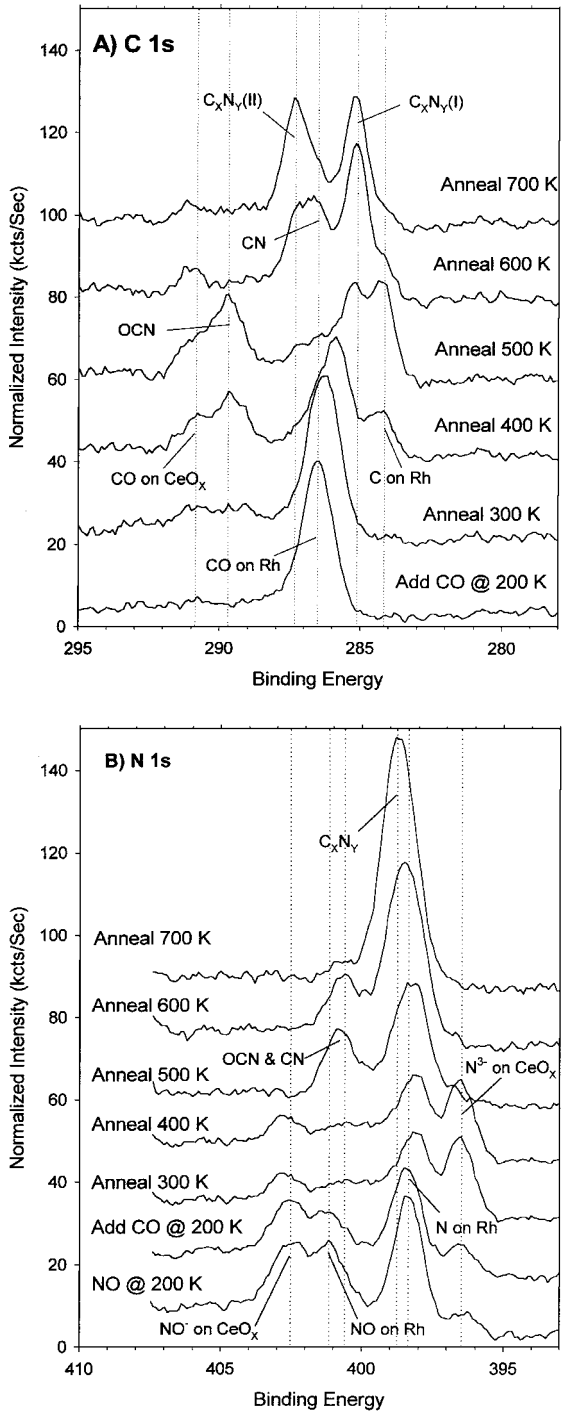

FIG. 4. (A) C 1*s* and (B) N 1*s* core-level photoemission spectra for sub-monolayer amounts of NO and CO adsorbed on Rh/CeO_x. The NO was adsorbed first at 200 K and then followed by CO at 200 K and progressively annealed as indicated.

TABLE 1

C 1*s* Peak Assignments

Binding energy	Assignment
284.0–284.4	Atomic C on Rh
285.3	C_XN_Y(I)
286.0–286.6	CO on Rh
286.7	CN
287.5	C_XN_Y(II)–(sp^3)
289.6	OCN
290.8–291.6	CO on CeO_x

The N 1*s* spectra following the adsorption of CO on a sub-monolayer coverage of NO on Rh/CeO_x are shown in Fig. 4b. The N 1*s* peak positions and assignments are summarized in Table 2. N^{3-}/CeO_x, N/Rh, NO/Rh, and NO^-/CeO_x are seen as they were in the absence of CO (Fig. 2b). The relative intensities of these peaks are different than those in Fig. 2b because of the lower NO coverage. The relative intensities of the different states for NO on CeO_x have been shown to be exposure dependent (18). Following CO adsorption at 200 K, there is little change in the N 1*s* spectrum except for an overall attenuation of the N 1*s* intensity. The origin of this attenuation, which persists to 500–600 K, is unknown.

A new feature between 400 and 401 eV appears after annealing between 400 and 500 K. The appearance of this feature coincides with the appearance of the OCN peak in the C 1*s* spectrum and is also assigned to OCN. Above 500 K the most prominent peak in the spectrum shifts from 398.1 to 398.7 eV, coinciding with the growth of C_XN_Y.

3.3. CO Adsorbed with N at 200 K

The co-adsorption of CO with N was examined and the results are shown in Figs. 5 and 6. N adsorbed on Rh was produced by exposing the sample to NO at 200 K, followed by annealing to 400 K to fully decompose the NO. Little, if any, NO is desorbed during this step. Following decomposition, it is assumed that the O migrates from the Rh to the ceria. Only one peak is observed in the O 1*s* spectrum (not shown), which is assigned to the O in CeO_x. In addition, the oxygen exchange following the decomposition and recombination of CO on Rh/CeO_x (12) and the thermodynamic stability of CeO_2 compared to O/Rh also suggest migration of the O from the Rh to the ceria.

TABLE 2

N 1*s* Peak Assignments

Binding Energy	Assignment
396.3	N^{3-} on CeO_x
397.9–398.3	Atomic N on Rh
398.3–398.8	C_XN_Y(I), C_XN_Y(II)
400.0–400.6	OCN, CN
401.1	NO on Rh
402.2–402.6	NO^- on CeO_x

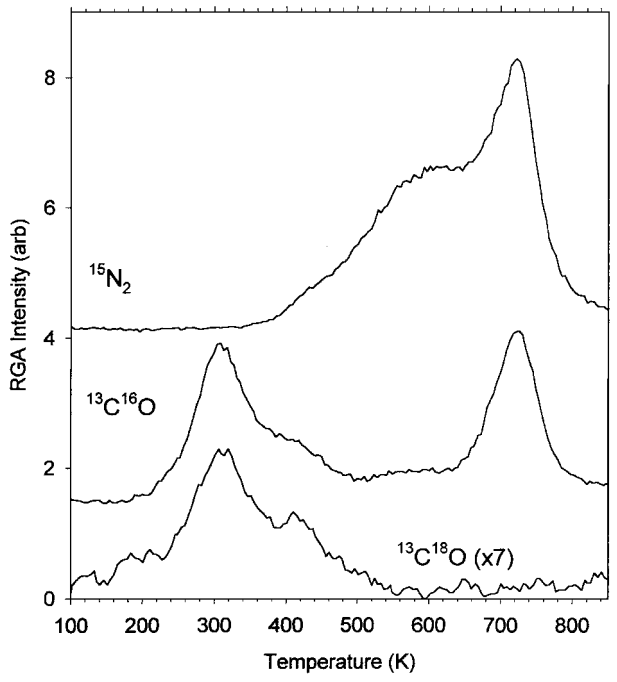

FIG. 5. Thermal desorption spectra for $^{13}C^{16}O$ adsorbed on dissociated $^{15}N^{16}O$ on Rh/CeO_x at 200 K. The $^{15}N^{16}O$ was adsorbed at 200 K and then annealed to 400 K. $^{13}C^{16}O$ was then adsorbed at 200 K. The $^{13}C^{18}O$ desorption is indicative of undissociated CO desorption.

After the NO was decomposed, the sample was exposed to CO at 200 K. The N layer did not block the adsorption of CO, unlike an NO layer, which does block CO adsorption (section 3.2). This result indicates that N and CO do not compete for the same sites. The resulting thermal desorption spectra are shown in Fig. 5. The highest temperature CO desorption state at 720 K is similar to that in Fig. 3. The desorption from 240 to 650 K can now be clearly divided into peaks at 300, 420, and 570 K. The $C^{13}O^{18}$ desorption indicates that the lowest two states are from undissociated CO and the highest two states are recombinative. More CO desorbs in this case than when CO is coadsorbed with NO. The extra CO desorbs in the undissociated states below 450 K. Part of the effect of pre-adsorbed N, therefore, is to block CO dissociation, which leads to more low-temperature undissociated desorption (compare Figs. 1 and 3).

The only major change in the N_2 desorption compared to that shown in Fig. 3 is the absence of the low-temperature state, which already desorbed prior to CO adsorption.

The C 1*s* and N 1*s* spectra following CO exposure on N-covered Rh/CeO_x are shown in Figs. 6a and 6b, respectively. The C/Rh peak, seen previously in Fig. 4a, does not occur. This suggests that the high coverage of atomic N blocks the decomposition of CO or that the reaction

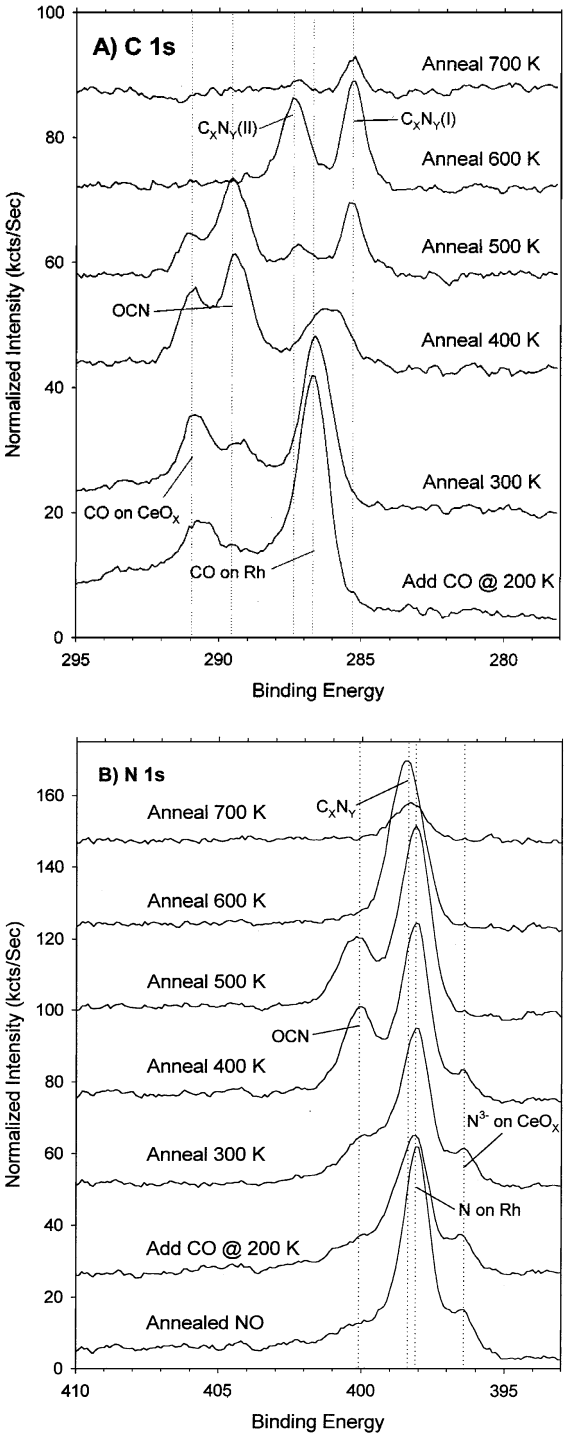

FIG. 6. (A) C 1*s* and (B) N 1*s* core-level photoemission spectra for CO adsorbed on dissociated NO on Rh/CeO_x at 200 K. The NO was adsorbed at 200 K and then annealed to 400 K. CO was then adsorbed at 200 K and progressively annealed as indicated.

of N with CO competes with the decomposition of CO. OCN first appears at 300 K and then increases as the temperature is increased until it disappears at 600 K. This is similar to what was observed following the co-adsorption of CO and NO. By 600 K the spectrum is composed of two well-resolved, symmetrically shaped peaks indicative of the C_XN_Y phase. The intensity of these two peaks decreases at a lower temperature compared to that shown in Fig. 4a. This decrease may be due to minor variations in the CeO_x oxidation state. Slightly more oxidized substrates destabilize the C_XN_Y.

The N 1*s* spectra consist of primarily N/Rh with a small amount of N^{3-} prior to CO adsorption. The addition of CO again attenuates the N 1*s* signal. OCN grows as the sample is heated, is intense at 400 and 500 K, and then disappears at 600 K. At 600 K only C_XN_Y is seen.

3.4. CO Adsorbed with N at 400 K

CO was adsorbed at 400 K on a N-covered surface in an effort to enhance the CO–N interaction. The Rh/CeO_x sample was exposed to NO at 200 K and then annealed to 400 K as shown in section 3.3. This surface was then exposed to CO at 400 K. The thermal desorption of CO and N_2 are shown in Fig. 7. Three CO desorption states are observed. The high-temperature recombinative state is indicative of the decomposition of C_XN_Y. Virtually all the N reacts with C eliminating the N_2 desorption between 500 and 600 K. The excess CO desorbs from an undissociated state at 470 K and a recombinative state at 580 K.

The C 1*s* and N 1*s* spectra are shown in Figs. 8a and 8b, respectively. Following CO exposure, OCN is very intense

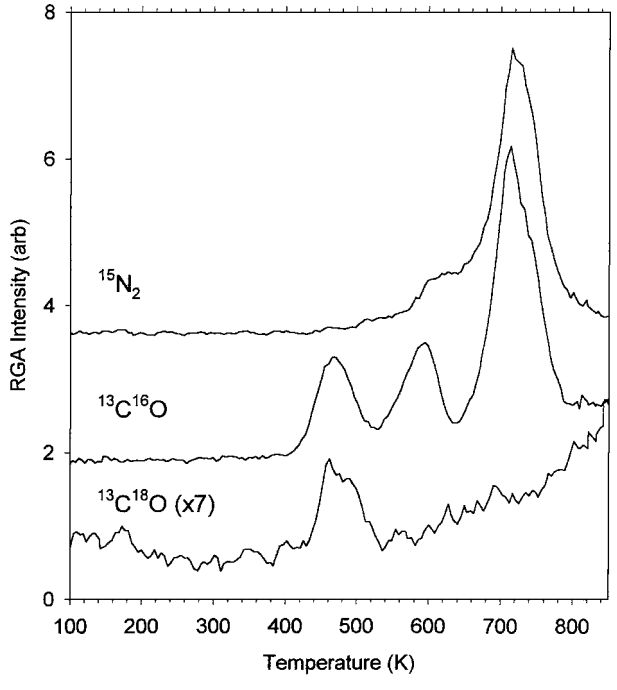

FIG. 7. Thermal desorption spectra for $^{13}C^{16}O$ adsorbed on dissociated $^{15}N^{16}O$ on Rh/CeO_x at 400 K. The $^{15}N^{16}O$ was adsorbed at 200 K and then annealed to 400 K. $^{13}C^{16}O$ was then adsorbed at 400 K. The $^{13}C^{18}O$ desorption is indicative of undissociated CO desorption.

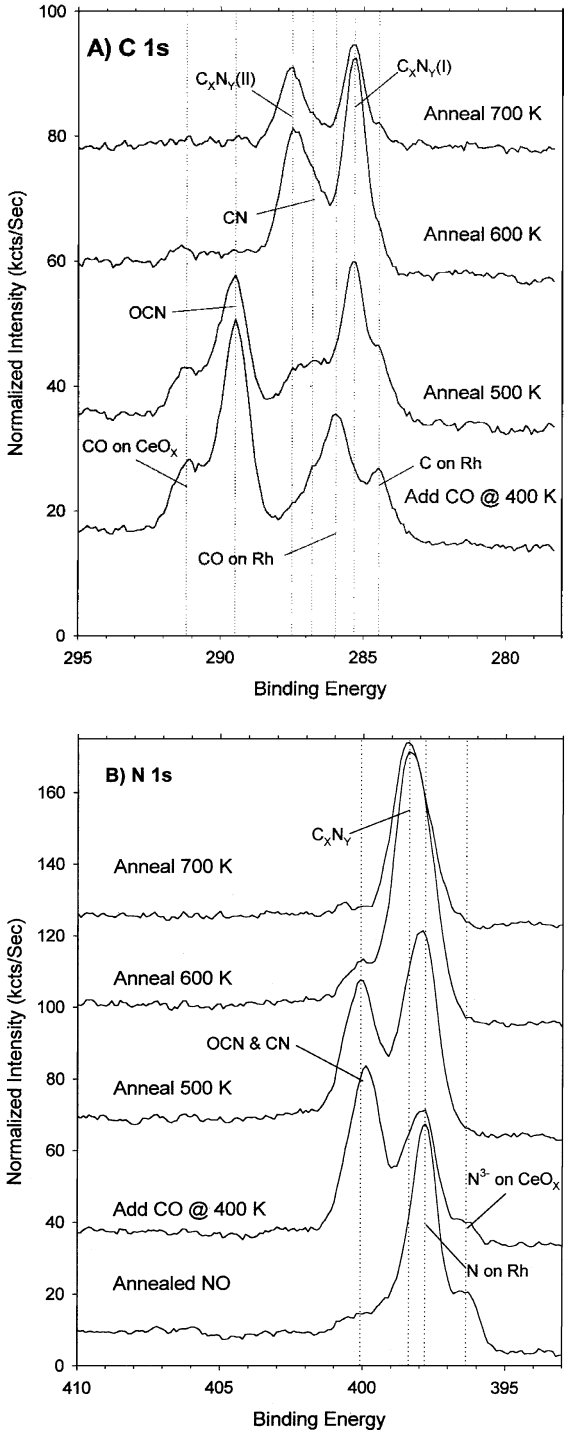

FIG. 8. (A) C 1*s* and (B) N 1*s* core-level photoemission spectra for CO adsorbed on dissociated NO on Rh/CeO_x at 400 K. The NO was adsorbed at 200 K and then annealed to 400 K. CO was then adsorbed at 400 K and progressively annealed as indicated.

in the C 1*s* spectrum. CO/Rh is also relatively intense and well resolved. CO/Rh is shifted to lower binding energy due to its lower coverage. Unlike the case when CO was adsorbed at 200 K, there is also an indication of atomic C formation. C_XN_Y formation is evident at 500 K while OCN and CO/Rh decrease. OCN and C/Rh disappear entirely at 600 K, and the asymmetry between 286 and 288 eV again indicates the presence of a third state near 287 eV. This third state disappears at 700 K, leaving the relatively symmetric pair of peaks.

After CO exposure at 400 K, there is more OCN than N/Rh evident in the N 1*s* spectrum (Fig. 8b). The intensity of the peak assigned to OCN is significantly reduced at 600 K but is still present. The OCN peak is absent in the C 1*s* spectrum at 600 K, however. This suggests that the peak at 400.1 eV may be associated with some other species in addition to OCN.

O 1*s* spectra were recorded to determine which adsorbed species also contain oxygen. The top spectrum in Fig. 9 was recorded after CO was adsorbed on Rh/CeO_x at 300 K without N or NO present. The intense peak at 530.9 eV is from the lattice O in CeO_x. The peak at 533 eV is assigned to CO/Rh. The bottom spectrum shows the O 1*s* spectrum following CO exposure to N-covered Rh/CeO_x at 400 K. The peak at 534.8 eV is assigned to OCN. There is a small amount of CO evident between the two main peaks. After the sample is annealed to 600 K, the middle spectrum is observed. The only peak evident is from the lattice O. This indicates that none of the adsorbed molecular species contain O at 600 K.

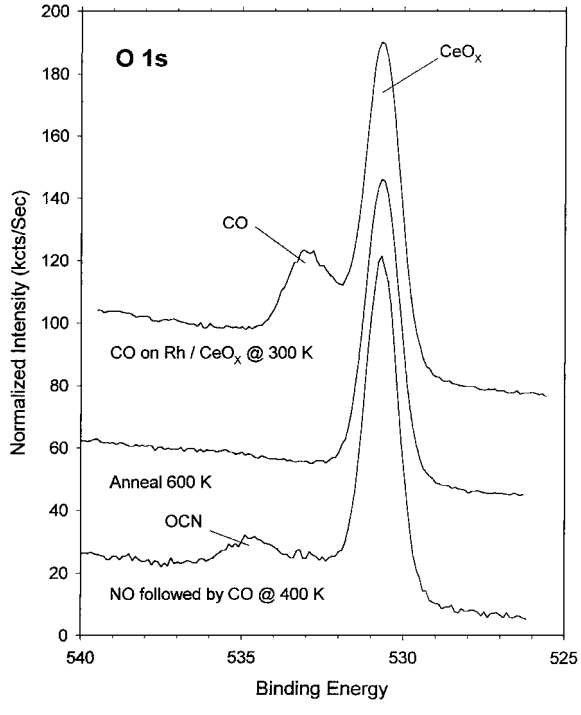

FIG. 9. O 1*s* spectra for CO adsorbed on dissociated NO on Rh/CeO_x at 400 K (bottom spectrum) and then annealed to 600 K (middle spectrum). For comparison, the top spectrum is from CO adsorbed by itself at 300 K on Rh/CeO_x.

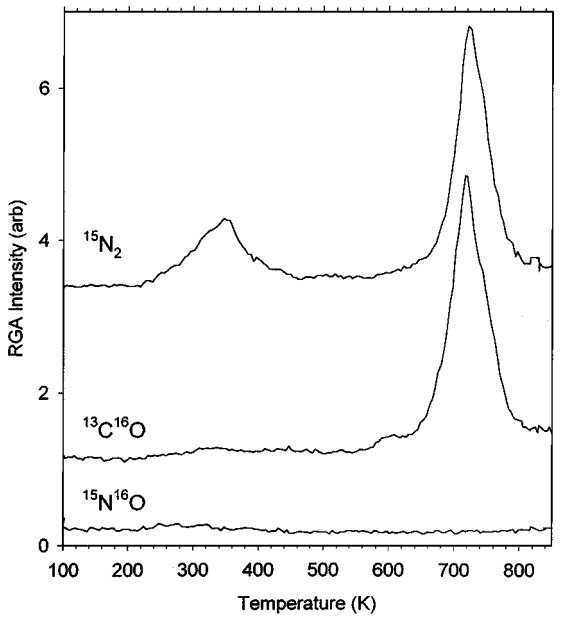

FIG. 10. Thermal desorption spectra for $^{15}N^{16}O$ adsorbed on dissociated $^{13}C^{16}O$ on Rh/CeO_x at 200 K. The $^{13}C^{16}O$ was adsorbed at 200 K and then annealed to 500 K. $^{15}N^{16}O$ was then adsorbed at 200 K.

3.5. NO Adsorbed with C at 200 K

CO was adsorbed on Rh/CeO_x at 200 K and then annealed to 500 K to produce a C-covered Rh surface. As shown in Fig. 1a, a small amount of CO may desorb in this step. NO was then adsorbed at 200 K. The CO and N_2 thermal desorption spectra are shown in Fig. 10. The CO and N_2 desorb simultaneously near 720 K. Essentially all the C and N react to form C_XN_Y. The N_2 desorption at 350 K comes from the dissociation and recombination of NO^- on CeO_x.

The C 1*s* and N 1*s* spectra for this system are shown in Figs. 11a and 11b, respectively. Following NO adsorption, the C 1*s* spectra are composed primarily of atomic C on Rh and CO on CeO_x for annealing temperatures up to 400 K. The atomic C signal is attenuated when the NO is adsorbed. This is similar to what happened to the atomic N signal when CO was adsorbed on N-covered Rh/CeO_x (Fig. 6b). At 500 K the atomic C is converted into CN and C_XN_Y. These conditions, i.e., the adsorption and annealing of NO on C-covered Rh/CeO_x, produce more CN in the C 1*s* and N 1*s* spectra than either CO + NO (Fig. 4) or CO + N (Fig. 6). There is only a small amount of OCN formed under these conditions.

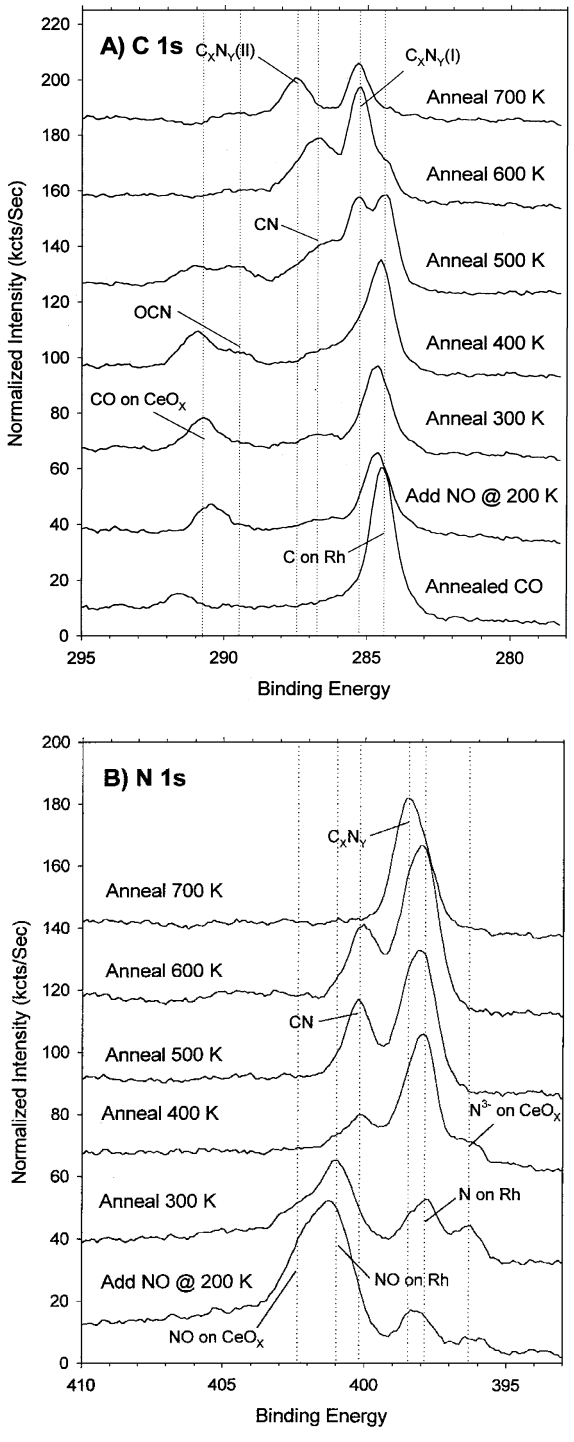

FIG. 11. (A) C 1*s* and (B) N 1*s* core-level photoemission spectra for NO adsorbed on dissociated CO on Rh/CeO_x at 200 K. The CO was adsorbed at 200 K and then annealed to 500 K. NO was then adsorbed at 200 K and progressively annealed as indicated.

4. DISCUSSION

4.1. Identification of Surface Intermediates

When CO and NO interact on Rh/CeO_x, seven distinct features are observed in the C 1*s* spectra and six features are observed in the N 1*s* spectra (Tables 1 and 2). Seven of these 13 features have been previously identified by examining CO (13) or NO (17, 18) by themselves on CeO_x and Rh/CeO_x (Fig. 2). C on Rh, CO on Rh, and CO on CeO_x are seen in the C 1*s* spectra, and N on Rh, NO on Rh, and NO^- and N^{3-} on CeO_x are seen in the N 1*s* spectra.

When NO and CO are co-adsorbed, new features appear in the SXPS spectra when the sample is annealed to 400 K. The C 1*s* peak at 289.6 eV, the N 1*s* peak at 400.1 eV, and the O 1*s* peak at 534.8 eV are assigned to isocyanate, OCN, for the following reasons. The intensities of these peaks correlate, appearing above 300 K and disappearing by 600 K. This indicates the presence of a species containing C, N, and O. The binding energy of the C 1*s* peak, 289.6 eV, indicates that the C atom has a large positive polarization. For comparison, CO on Rh is at 286.4 eV and CO on CeO_x, which likely forms a carbonate, CO_3^{2-}, or a carboxylate, CO_2^{2-}, is at 291 eV. Adsorption of CO_2 on CeO_x produces a C 1*s* peak at 290.5 eV (19). The species associated with the 289.6-eV peak has a binding energy similar to that of CO_2 or carbonate but also contains N. This feature is the most intense when CO reacts with N/Rh at 400 K (Fig. 8) but is not formed when NO reacts with C/Rh (Fig. 11). OCN can form directly from CO + N but requires breaking the N–O bond to form from NO + C.

It is not clear whether the OCN is located on the Rh or on the oxide. The stability of the species suggests that it is probably on the oxide. OCN on Rh(111) decomposes below 400 K (20). The reduction of NO by CO on Rh supported on silica forms OCN on both the Rh and the silica (9, 10). The OCN was stable on the silica at 515 K but disappeared on the Rh (10). This was demonstrated by vibrational spectroscopy where ν_a(NCO) is between 2250 and 2300 cm^{-1} if the isocyanate is on the oxide and is between 2150 and 2200 cm^{-1} if it is on the metal. EELS or IR would similarly show whether the OCN is on the Rh or on the ceria in the present system.

When the sample is annealed to 600 K, the isocyanate disappears from the C 1*s* spectra. The only peak present in the O 1*s* spectrum is the lattice oxygen feature from the CeO_x. The molecular fragments remaining on the surface therefore contain only C and N.

There is not enough information in the C 1*s* and N 1*s* XPS spectra to uniquely identify the species on the surface above 600 K. However, the peak positions do provide some insight into the nature of the adsorbed species. The XPS spectra of C_XN_Y species have been extensively studied with respect to the characterization of carbon nitride thin films (21–24). Although there is some disagreement as to peak assignments, the following characteristics are generally agreed upon in the analysis of the spectra. Highly polarized bonds result in large positive shifts in the C 1*s* binding energies and smaller negative shifts in the N 1*s* binding energies. C–N bonds exhibiting sp^3 hybridization are the most polarized (23). Conversely, sp^2 hybridization will produce less polarization and smaller shifts. This behavior is evident in the XPS spectra of pyridine (C_5H_5N) in which the atoms are sp^2 hybridized and urotropine ($C_6H_{12}N_4$) where the atoms have an sp^3 hybridization (21). The extent of the positive shift in the C 1*s* binding energy is also directly related to the number of N atoms bonded to the C. The binding energies for *sp*-hybridized atoms (–C≡N) lie inbetween those for sp^3 and sp^2 species based on the XPS spectra of polyacrylonitrile (24), but lie closer to the sp^3 positions.

Above 600 K, three peaks occur in the C 1*s* spectra and two peaks occur in the N 1*s* spectra. Following the analysis presented above, the highest binding energy peak in the C 1*s*, C_XN_Y(II) at 287.5 eV, is assigned to sp^3-hybridized C bonded to one or more N atoms. This peak is associated with the N 1*s* peak at 398.5 eV.

The next lowest binding energy peak at 286.7 eV in the C 1*s* spectra is shifted by less than a volt compared to the feature assigned to the sp^3-hybridized C. It is therefore reasonable to assign this peak to a –C≡N species. Above 500 K, the intensity of this peak is directly correlated with the intensity of the peak at 400.1 eV in the N 1*s* spectra. The 400.1-eV feature is therefore assigned to two species, OCN and –C≡N. These species are clearly distinguished from each other by the effect of annealing and the presence of O in the fragment. OCN is present between 400 and 500 K while –C≡N exists primarily between 500 and 600 K. The C 1*s* and N 1*s* peak positions are similar to those in polyacrylonitrile (24) but are much higher than the positions reported for CN on Pd(110) (25), Ni(110) (26), and Rh(110) (27). However, the peak positions for NO and N on the small Rh particles are also greater than the positions of NO and N on single-crystal Rh (3, 28). The shift to higher binding energy may be the result of reduced final state screening on the small particles.

Finally, the C_XN_Y(I) peak in the C 1*s* spectra at 285.3 eV is the most difficult to assign. The low binding energy would indicate that it corresponds to C which is not polarized significantly. There is no corresponding peak at higher binding energy in the N 1*s* spectrum. The peak at 398.5 eV in the N 1*s* spectra appears to be associated with both C_XN_Y(I) and C_XN_Y(II) in the C 1*s* spectra. There are several possible assignments for C_XN_Y(I). The C 1*s* binding energy shifts to progressively higher binding energy as the C is bound to more N atoms. The C_XN_Y(I) could therefore be C attached to one N atom while C_XN_Y(II) is from C bound to two or more N atoms. The number of N neighbors affects the C 1*s* binding energy but does not affect the N 1*s* binding energy (23). Hence, the single N 1*s* peak can be associated with two C 1*s* peaks. The biggest problem with this assignment is the magnitude of the difference between the two C 1*s* peaks, i.e., >2 eV. This difference appears to be too large to be induced by a variation in the number of N neighbors (23).

An alternative assignment for C_XN_Y(I) is that it is associated with C bonded just to other C atoms. The bonds between these atoms would be unpolarized; however, their binding energy would be slightly higher than the binding energy of a single C atom. A single C atom is better able to withdraw charge from the metal particle. The single peak

in the N 1*s* spectra would then only be associated with C_XN_Y(II). Ronning *et al.* assigned the lowest binding energy C 1*s* state in their spectra to sp^3 C bonded only to other C atoms or to a very low concentration of N (23). It is difficult to imagine why this diamond-like state would form only in the presence of N on Rh/CeO_x. When the N is not present, atomic C recombines with O and desorbs as CO around 600 K (Fig. 1). In addition, the presence of C bound primarily to other C implies an excess of C compared to N. The thermal desorption indicates that the opposite is the case. CO and N_2 desorption near 700 K have similar intensities. Therefore, the N : C ratio is roughly 2 : 1.

In summary, the SXPS spectra indicate that the interaction between NO and CO on Rh/CeO_x first forms OCN as the sample is heated. This is followed by the decomposition of OCN and the production of a variety of C_XN_Y fragments consisting of different numbers of N bound to each C atom and/or different hybridizations in the C–N bonding.

4.2. Mechanistic Implications

CO and NO react on single-crystal Rh in UHV to form N_2 and CO_2 as described by reactions [1.1]–[1.5]. Isocyanate and carbon–nitrogen compounds are not typically observed and are not considered significant reactions in the overall mechanistic understanding (8). Similar chemistry is observed in the present study when CO and NO are adsorbed on Rh on fully oxidized CeO_2 (19). N_2, NO, CO, and CO_2 are observed in thermal desorption in a manner similar to the reaction of NO and CO on single-crystal Rh (2). The C 1*s* and N 1*s* spectra further indicate that the only surface species are NO, CO, and N.

The reaction results change considerably if the ceria substrate is reduced. The reaction pathway for NO and CO coadsorbed at 200 K on Rh/CeO_x and then annealed to higher temperatures is summarized in Fig. 12. No NO or CO_2 are desorbed, the N_2 and CO desorb at very high temperatures, and isocyanate and C_XN_Y are detected on the surface. These results can be explained in the following way. Reduced ceria is very effective in removing O from the Rh particles (reaction [1.9]). This effectively removes O as a reactant. As a result, CO_2 production will be inhibited (reaction [1.5]) and NO decomposition will be promoted (reaction [1.3]). Ordinarily, the reaction of CO + O is favored compared to the reaction of CO + N (reaction [1.6]). However, when the O reactant is removed, the CO + N channel becomes predominant. The amount of isocyanate is the greatest when CO is reacted with atomic N at 400 K (Fig. 8a). This is because the availability of excess CO allows the production of more OCN. When the CO is adsorbed with atomic N at lower temperatures, the OCN formation is limited by CO desorption (reaction [1.2]).

The isocyanate decomposition mechanism is not clear. It may decompose to produce desorbed CO or atomic C on the surface. The isocyanate disappears between 500 and 600 K (Figs. 4a and 8a). There is a CO desorption peak in this temperature range (Fig. 7), but only $^{13}C^{16}O$ and not $^{13}C^{18}O$ is produced. This indicates either that the isocyanate decomposes to atomic C, which then reacts with lattice O to produce CO, or that the isocyanate forms a complex with the CeO_x and then abstracts oxygen from the CeO_x upon decomposition.

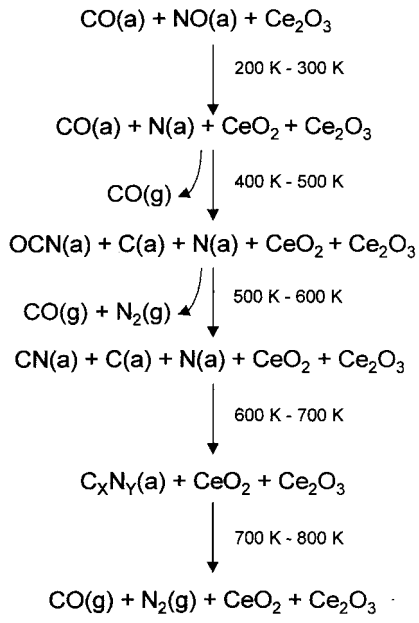

FIG. 12. The reaction pathway for NO + CO co-adsorbed on Rh/CeO_x at 200 K. The reaction of CO + N would enter the pathway at Step 2, while the reaction of NO + C would enter the pathway at Step 4.

C can also be produced through the decomposition of CO on Rh on reduced ceria (reaction [1.8]) (11–13). The C can react with N to produce C_XN_Y species. These species are evident in the C 1*s* and N 1*s* spectra at elevated temperature (>600 K). The C_XN_Y species are apparently more stable than isolated C and N on the Rh particles. Following C_XN_Y decomposition, CO and N_2 are produced at higher temperatures than those observed when CO and NO are adsorbed separately.

The current results provide clues that allow us to predict what will happen when NO reacts with a hydrocarbon on this surface. The reaction of NO with C_2H_4 has been studied on Rh(111) (29). This system produces H_2, NO, CO, CO_2, H_2O, HCN, and N_2. Because the reduced ceria removes the O from the Rh, we would expect that NO, CO_2, and H_2O would not be observed on Rh/CeO_x. Ethylene largely decomposes by 400 K on Rh(111). The co-adsorption of NO and ethylene on Rh/CeO_x should yield primarily C and N and should behave like the reaction of NO with C as described in section 3.5. We cannot predict what effect H will have or whether HCN will be produced.

The reaction of NO + C_2H_4 on Rh on fully oxidized CeO_2 is potentially more complex. Since O is not removed from

the Rh by the CeO_2, we might expect that Rh/CeO_2 will behave similarly to Rh(111) (29). However, Ferriz *et al.* have shown that ethylene on Rh/CeO_2 produces CO and CO_2 (30). This demonstrates that C on the Rh can abstract O from the CeO_2. Oxygen-containing products may therefore be more prevalent from Rh/CeO_2 than from Rh(111).

Experiments are underway to determine the interaction between NO and C_2H_4 on Rh/CeO_x.

CONCLUSIONS

The interaction between CO and NO on Rh/CeO_x is dramatically different compared to the interaction between CO and NO on single-crystal Rh. As the NO decomposes when the sample is heated, the CeO_x removes the O from the Rh particles. The absence of free O on the Rh results in the loss of CO_2 desorption and the formation of OCN on the surface. In addition, Rh/CeO_x is more active than single-crystal Rh and is able to dissociate CO. The C and N react to form stable C_XN_Y species that decompose near 700 K. The N desorbs as N_2 and the C reacts with lattice O to produce CO.

ACKNOWLEDGMENTS

This research was sponsored by the Division of Chemical Sciences, Geosciences, and Biosciences, Office of Basic Energy Sciences, U.S. Department of Energy, under contract DE-AC05-00OR22725 with Oak Ridge National Laboratory, managed and operated by UT-Battelle, LLC. The National Synchrotron Light Source, Brookhaven National Laboratory, is supported by the U.S. Department of Energy, Division of Materials Sciences and Division of Chemical Sciences.

REFERENCES

1. Campbell, C. T., and White, J. M., *Appl. Surf. Sci.* **1**, 347 (1978).
2. Root, T. W., Schimdt, L. D., and Fisher, G. B., *Surf. Sci.* **150**, 173 (1985).
3. Peden, C. H. F., Belton, D. N., and Schmieg, S. J., *J. Catal.* **155**, 204 (1995).
4. Belton, D. N., and Schmeig, S. J., *J. Catal.* **144**, 9 (1993).
5. Schmatloch, V., Jirka, I., Heinze, S., and Kruse, N., *Surf. Sci.* **331**, 23 (1995).
6. Schmatloch, V., and Kruse, N., *Surf. Sci.* **269/270**, 488 (1992).
7. Dubois, L. H., Hansma, P. K., and Somorjai, G. A., *J. Catal.* **65**, 318 (1980).
8. Zhdanov, V. P., and Kasemo, B., *Surf. Sci. Rep.* **29**, 31 (1997).
9. Hecker, W. C., and Bell, A. T., *J. Catal.* **85**, 200 (1984).
10. Hecker, W. C., and Bell, A. T., *J. Catal.* **85**, 389 (1984).
11. Stubenrauch, J., and Vohs, J. M., *J. Catal.* **159**, 50 (1996).
12. Stubenrauch, J., and Vohs, J. M., *Catal. Lett.* **47**, 21 (1996).
13. Mullins, D. R., and Overbury, S. H., *J. Catal.* **188**, 340 (1999).
14. Overbury, S. H., Mullins, D. R., Huntley, D. R., and Kundakovic, Lj., *J. Phys. Chem*. **103**, 11308 (1999).
15. Mullins, D. R., Radulovic, P. V., and Overbury, S. H., *Surf. Sci.* **429**, 186 (1999).
16. Mullins, D. R., Overbury, S. H., and Huntley, D. R., *Surf. Sci.* **409**, 307 (1998).
17. Overbury, S. H., and Mullins, D. R., submitted for publication.
18. Overbury, S. H., Mullins, D. R., Huntley, D. R., and Kundakovic, Lj., *J. Catal.* **186**, 296 (1999).
19. D. R. Mullins, unpublished results.
20. Kiss, J., and Soloymosi, F., *Surf. Sci.* **135**, 243 (1983).
21. Marton, D., Boyd, K. J., Al-Bayati, A. H., Todrov, S. S., and Rabalais, J. W., *Phys. Rev. Lett.* **73**, 118 (1994).
22. Fujimoto, F., and Ogata, K., *Jpn. J. Appl. Phys.* **32**, L420 (1993).
23. Ronning, C., Feldermann, H., Merk, R., Hofsäss, H., Reinke, P., and Thiele, J.-U., *Phys. Rev. B* **58**, 2207 (1998).
24. Scharf, T. W., Ott, R. D., Yang, D., and Barnard, J. A., *J. Appl. Phys.* **85**, 3142 (1999).
25. Baraldi, A., Lizzit, S., Ramsey, M. G., and Netzer, F. P., *Surf. Sci.* **416**, 214 (1998).
26. Blyth, R. I. R., Kardinal, I., Netzer, F. P., Ramsey, M. G., Chrysostomou, D., and Lloyd, D. R., *Surf. Sci.* **415**, 227 (1998).
27. Bondino, F., Baraldi, A., Comelli, G., and Netzer, F. P., submitted for publication.
28. Lizzit, S., Baraldi, A., Cocco, D., Comelli, G., Paolucci, G., Rosei, R., and Kiskinova, M., *Surf. Sci.* **410**, 228 (1998).
29. van Hardeveld, R. M., Schmidt, A. J. G. W., and Niemantsverdriet, J. W., *Catal. Lett.* **41**, 125 (1996).
30. Ferriz, R. M., Egami, T., and Vohs, J. M., *Catal. Lett.* **61**, 33 (1999).